Light rays and wave fronts in strong gravity

V. Karas[1], Y. Kojima[2] and D. Kunneriath[3]

[1] *Astronomical Institute of the Czech Academy of Sciences,*
Boční II 1401, CZ-14100 Prague, Czech Republic
(E-mail: vladimir.karas@cuni.cz)

[2] *Department of Physics, Hiroshima University, Higashi-Hiroshima,*
Hiroshima 739-8526, Japan

[3] *National Radio Astronomy Observatory, 520 Edgemont Road,*
Charlottesville 22903 (VA), USA

Abstract. Accretion onto black holes often proceeds via an accretion disk or a temporary disk-like pattern. Variability features observed in light curves as well as theoretical models of accretion flows suggest that accretion disks tend to be inhomogeneous – variety of substructures (clumps) emerge within the flow. Rapid orbital motion of individual clumps then modulates the observed signal in X-rays. Furthermore, changes of spectral lines and polarization properties of the observed signal (or the absence of changes) constrain the models and reveal information about general relativity (GR) effects. In this write-up we summarize the basic equations that have been employed to study light propagation near black holes and to derive the radiation signal that can be expected at a detector within the framework of geometrical optics approximation.
Key words: Black holes – Accretion, accretion disks – General relativity

1. Introduction

Accreting black holes are thought to be the most likely agents driving active galactic nuclei and compact binaries. Nonetheless, various aspects of the picture still need to be understood and several viable alternatives have been proposed (see, e.g., an overview in Eckart et al., 2017). Numerical and semi-analytical computations of emission continua and emission-line profiles are important tools for verification of models with black-hole accretion disks (Gerbal & Pelat, 1981; Fabian et al., 1989; Kojima, 1991; Laor, 1991; Karas et al., 1992). Here we briefly outline the underlying ideas, believing that the disk radiation must be affected by the orbital motion of its elements. An intrinsically narrow spectral line with a single, well-defined peak in the local rest frame co-moving with the disk material becomes broader or it can be split into more components in the frame of a distant observer. This has to be modelled in a manner consistent with the underlying continuum, taking into account the interplay of parameters describing the system (Fabian et al., 2000).

We adopt the standard black-hole accretion disk scenario (Frank et al., 1992), where the radiation signal emerges from the surface of the disk along the range of radius, $R_{\rm in} < R < R_{\rm out}$. Because of the temperature profile, the main contribution to the bulk emissivity of low ionization lines originates in the distant region of $\approx 10^4 R_{\rm g}$, i.e. near $R_{\rm out}$.[1] In addition, there is Doppler-boosted radiation coming from $R \approx R_{\rm in}$. As a result, two peaks appear in the line profile. Assuming Keplerian rotation, the orbital velocity corresponding to these peaks satisfies the relation

$$\frac{v_{\rm K|R=R_{\rm in}}}{v_{\rm K|R=R_{\rm out}}} \simeq \sqrt{\frac{R_{\rm out}}{R_{\rm in}}}, \tag{1}$$

which is independent of the disk inclination angle. This ratio gives us the first estimate of the disk size (GR effects will modify this to certain extent). Typically, for $M \approx M_\odot$ one obtains $R_{\rm out} \approx (10^4\text{–}10^5) R_{\rm g}$. The observer view angle has to be determined independently.

A direct consequence of predominantly azimuthal motion of the radiating matter is the onset of a double-peaked line core, as in a self-absorbed line. Near the inner rim of the accretion flow the velocity of the bulk motion grows and it becomes comparable with the speed of light. Naturally, fast motion leads to the spectral-line broadening. However, double-peaked profiles are only rarely observed (Chen & Halpern, 1989; Eracleous & Halpern, 1994): the lines are usually filled in. This is also the evidence for large $R_{\rm out}$. On the other hand, general-relativistic light-bending and the significant frequency shifts arise at small radii, in the immediate neighbourhood of the black-hole horizon, and they also contribute to the line asymmetry and broadening (Kojima, 1991; Laor, 1991; Kojima & Fukue, 1992; Karas et al., 1995).

The Doppler effect transforms photons of radiation emitted at wavelength $\lambda_{\rm em}$ to the observed wavelength

$$\lambda_{\rm obs} = \lambda_{\rm em} \frac{(1 - \beta y)}{\sqrt{1 - \beta^2}} \approx \lambda_{\rm em} \left(1 + \frac{1}{2}\beta^2 - \beta y \right), \tag{2}$$

where $\beta = v/c$, $y = \sin\phi \sin\theta_{\rm obs}$ (ϕ is the azimuthal coordinate in the disk plane and $\theta_{\rm obs}$ is the inclination of the observer). Analogously, the gravitational redshift is

$$\lambda_{\rm obs} = \frac{\lambda_{\rm em}}{1 - \beta^2}. \tag{3}$$

The position of the centroid of the line is independent of the disk inclination. Naturally, one cannot separate Doppler and gravitational shifts in a complete, self-consistent relativistic treatment of the problem. The centroid wavelength depends on inclination, when the wavelength shift, anisotropic emissivity of the

---

[1] The Schwarzschild radius $R_{\rm g}$ is defined in terms of the black hole mass $M_\bullet$: $R_{\rm g} \equiv 2GM_\bullet/c^2 \sim 3 \times 10^{13} M_8$ cm, where $M_8 = M_\bullet/10^8 M_\odot$ and $M_\odot$ denotes the mass of the Sun. $R_{\rm g}$ defines the linear size of a non-rotating black hole, whereas a maximally rotating (Kerr) black hole has the size half $R_{\rm g}$.
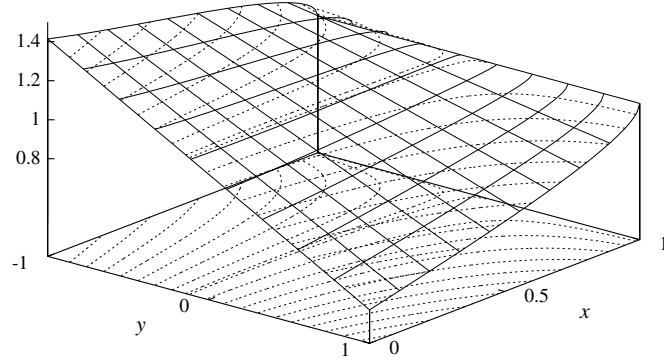
Figure 1. Redshift function $g(x, y)$ in dependence on two dimensionless spatial coordinates within the disk plane, $y = \sin\phi \sin\theta_{\mathrm{obs}}$ and $x = 1 - 3R_{\mathrm{g}}/R$. Different components of the overall energy shift add up to produce energy decrease ($g > 1$) or enhancement ($g < 1$) in different regions of the disk. This definition of (x, y) allows us to capture the entire disk plane from circular photon orbit at $r = 3R_{\mathrm{g}}$ up to infinity, $r \to \infty$ (Murphy et al., 2009).

material depending on the emission angle, and gravitational focusation of light rays are properly taken into account.

2. Calculating the observed spectral line profiles

The radiation originating from the gaseous elements at the inner edge of the disk experiences stronger gravitational and transverse Doppler redshift than the radiation from regions located further out. This results in a redward asymmetry of the skewed line. In addition, the Doppler-boosted radiation from the approaching material contributes to an enhanced peak of the blue wing of the line. Elements of the ring emit radiation with frequency $\nu = \nu_{\mathrm{em}}$ that represents the Dirac δ-function in the local rest frame. The line profile results from a superposition of individual contributions affected by a competition of the overall Doppler effect and the gravitational redshift. This observed profile depends on the inclination θ_{obs}. For the case of a disk, the line profile can be obtained by splitting the disk into a number of concentric rings, each emitting with its own local frequency and intensity, and summing their total radiation together.

Graphs of the relative frequency shift (the redshift factor)

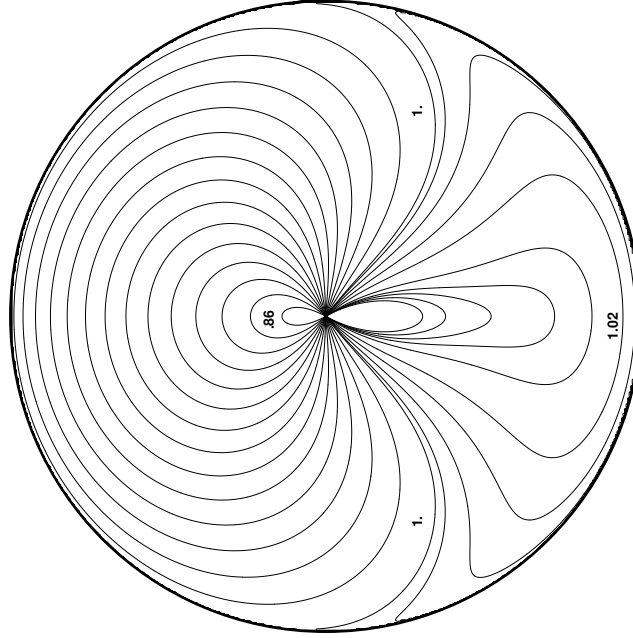$$1 + z \equiv g \equiv \frac{\lambda_{\mathrm{obs}}}{\lambda_{\mathrm{em}}} \tag{4}$$

Figure 2. Isocontours of g in the disk surface – a projection along the disk axis. Radial coordinate of the circle (x) is defined as in the previous figure, the azimuthal coordinate is ϕ here. A distant observer is located on the right side of the disk with a fixed value of view angle inclination, $\theta_{\mathrm{obs}} = 15\,\mathrm{deg}$. Values of $g > 1$ and $g < 1$ correspond to redshifted and blueshifted radiation, respectively.

along the Keplerian disk surface are shown in figures 1–2, taking into account general relativistic effects on the radiation. The formula (4) can be rewritten in a simpler form within the pseudo-Newtonian approximation,

$$g = \sqrt{\frac{R - 2R_{\mathrm{g}}}{(R - 3R_{\mathrm{g}})\,R}} \left(\sqrt{R - 2R_{\mathrm{g}}} - y \right). \tag{5}$$

The formula (5) is valid for a non-rotating black hole, however, a more complicated expression can be derived also in the rotating (Kerr) case, where it depends on the black-hole spin (and thus it enables to constrain the black hole rotation by fitting the observed spectra). An algorithm for the calculation of the predicted effects in spectral line profiles has been implemented in variety of modifications and under various assumptions (see Karas, 2006, and references cited therein). It can be outlined in a few steps as follows. Let us remind the reader that we assume the approximation of geometrical optics ($\lambda \ll R_{\mathrm{g}}$).
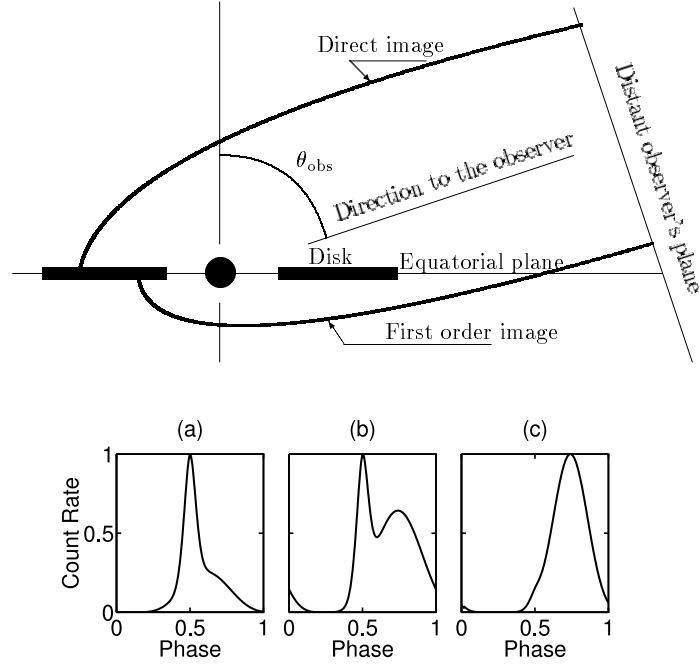
Figure 3. Top: a schematic illustration of the arrangement for a simulated image of the black-hole accretion disk, shown here in the poloidal cross-section. Bottom: Typical light-curves from a spot orbiting over one complete revolution on the surface of an accretion disk. Parameters: (a) $r = 3R_g$, $\theta_{obs} = 80$ deg (lensing peak dominates the lightcurve near the orbital phase 0.5); (b) $r = 44R_g$, $\theta_{obs} = 80$ deg; (c) $r = 44R_g$, $\theta_{obs} = 20$ deg (Doppler peak dominates near the phase 0.75). For further details, see Karas & Kraus (1996); Dovčiak et al. (2004); Karas (2006).

Firstly, we calculate (or define) the disk surface, $z \equiv z(R)$, and determine the intensity of radiation $I^R(R)$ which is emitted from the surface as a function of radius, frequency of radiation and direction with respect to the disk surface in the frame co-rotating with the disk material. As we saw earlier, in the simplified formulation of the standard model one assumes thermal radiation with an isotropic distribution in all directions arising from the equatorial plane, $z = 0$, but the problem becomes much more complex if it is to be solved self-consistently with the equation of radiative transfer. In vacuum, wave fronts of emerging radiation can be solved via the eikonal equation, which in the Schwarzschild metric reads (Hanni, 1977)

$$-\left(1 - \frac{2M}{r}\right)(\psi_{,r})^2 + \left(1 - \frac{2M}{r}\right)^{-1}(\psi_{,t})^2 - r^{-2}(\psi_{,\phi})^2 = 0. \qquad (6)$$
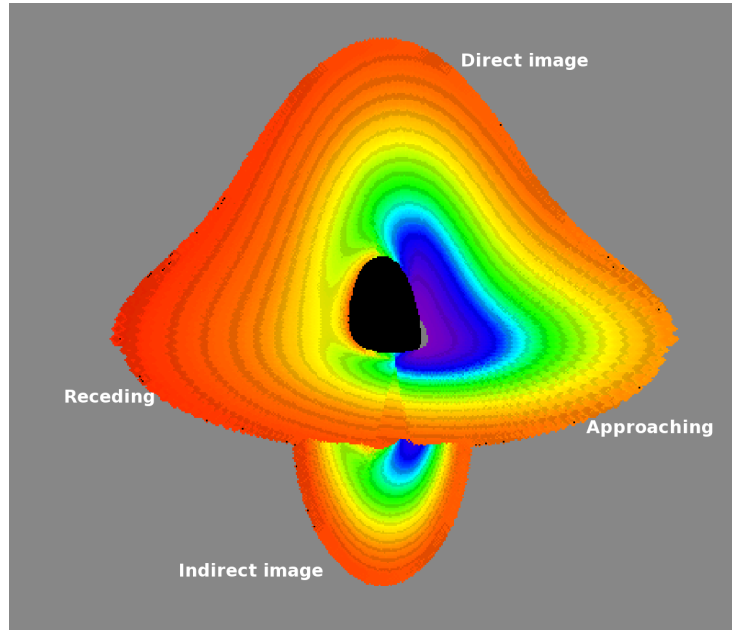
Figure 4. A synthetic image of a thin disk as projected onto the detector plane and viewed by a distant observer; the case of a rotating black hole in the center (colour coded by energy of photons at the detector plane; $a/M = 0.99$, $\theta_{\mathrm{obs}} = 85$ deg). The inner rim has been set at the innermost stable circular orbit (ISCO), while the outer radius is set at a somewhat arbitrary value. Part of the direct image from the region of the disk behind the central object with respect to the observer acquires a significant distortion and it appears to be elevated more above the equatorial plane. In addition, the observer can also see the first order (indirect) image, which has been formed by the rays crossing the equatorial plane once (in the bottom part of the picture). The contribution of the first and the higher order images to the total radiation flux depends on inclination of the distant observer, optical thickness of the disk, and a number of other parameters. The colour scale ranges from $g = 0.6$ (blue, the approaching side) to $g = 1.4$ (red, the receding part), corresponding to energy blueshift and redshift of the emerging photons, respectively; see fig. 5 for a different representation of the redshift function across the disk plane.

Eq. (6) can be solved by separation of variables, $\psi(t, r, \phi) \equiv R(r) + \alpha\phi - \omega t$. Photon propagation in the vacuum curved spacetime can be formally represented in terms of wave fronts $\psi = \mathrm{const}$ distorted by the influence of material media in the flat spacetime. Also in Kerr metric the wave fronts can be defined and solved analytically, however, the structure of the eikonal equation is more complicated because of frame dragging.
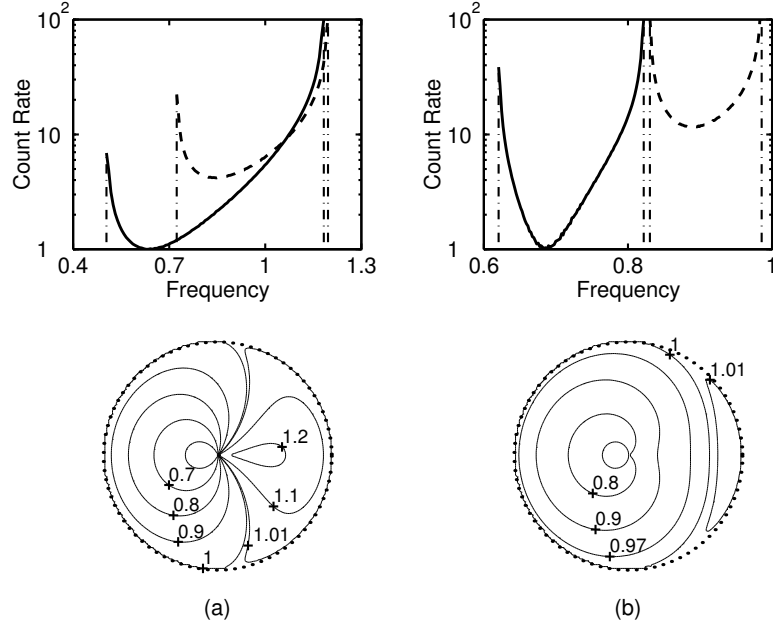
Figure 5. The range and the distribution of the redshift function across the equatorial accretion disk. Lower panels: lines of equal value of frequency shift g on a disk in Keplerian rotation around a Schwarzschild black hole, constructed in a way similar to fig. 2: an observer looks from the bottom of the page ($\phi = 0$). and both plots are drawn with the radial coordinate $x \equiv 1 - 3\,R_\mathrm{g}/r$ ($0 \leq x \leq 1$). Values of g-factor are indicated in the figure. The whole equatorial plane outside the inner edge of the disk is thus captured in this illustration; dotted circles correspond to $x = 1$. Observer inclination is (a) 85 deg (almost edge-on view), and (b) 20 deg (almost pole-on view). Upper panels: The corresponding observed photon count rates, i.e., the incoming photon flux (in arbitrary units) from a point-like source orbiting in the disk plane at $r_\mathrm{em} = 3R_\mathrm{g}$ (solid line) and $r_\mathrm{em} = 8R_\mathrm{g}$ (dashed line), averaged over the entire revolution. Effectively, the shape represents an observed profile of an narrow emission ring of a given radius emitting intrinsically at a single frequency $\nu = \nu_\mathrm{em}$. This shows how the photon energy is influenced by strong gravity of the black hole at different location of the accretion disk. The count rate is in arbitrary units and the frequency is normalized to the unit emission frequency ($\nu_\mathrm{em} = 1$; see Karas & Kraus, 1996, for further details).

Let us note at this point that for definiteness of examples and illustration purposes we adopt the standard (relativistic) black-hole accretion disk scenario (Frank et al., 1992; Kato et al., 2008), where the locally emitted spectrum is de-

scribed by multi-temperature thermal radiation (a superposition of black body spectra with the temperature changing as a function of radius). Also, we remind the reader that our discussion concerns only the gravitational effects on the light rays that propagate through empty (curved) space-time of the black hole. In the other words, the entire volume above the accretion disk is treated as optically thin. A more realistic description will require to take the scattering effects on the photon propagation into account in the disk corona.

Secondly, we have to specify location of a distant observer with respect to the disk axis. In the usual notation, inclination angle of $\theta_{\mathrm{obs}} = 90 \deg$ means edge-on view while $\theta_{\mathrm{obs}} = 0 \deg$ means pole-on view. Distant observer's plane (i.e., a "detector plane") is perpendicular to the direction $\theta = \theta_{\mathrm{obs}}$ at an infinite spatial distance from the source. One has to choose a convenient integration grid within the disk surface if the integration is to be carried out numerically.

Each grid point (image pixel) determines unambiguously a photon ray that crosses the plane of the observer perpendicularly (fig. 3). We calculate intersections of these rays with the disk surface $z \equiv z(R)$. Photon trajectories (null geodesics) will not be straight lines in space if effects of general theory of relativity are taken into account but this fact poses only a technical complication in calculating the intersections rather than a principal difference. Therefore, thirdly, we transform radiation intensity from the local disk frame, $I^{\mathrm{R}}(R, z(R); \nu^{\mathrm{R}}, \mu^{\mathrm{R}})$, to the observer's laboratory frame, $I^{\mathrm{L}}(R, z(R); \nu^{\mathrm{L}}, \mu^{\mathrm{L}})$, and propagate the intensity to the observer's plane. As mentioned above, a typical double-horn profile arises in the observed spectral line (although only one peak may be seen for some parameter values, namely, the inclination angle and the emission radius). Finally, we calculate the total observed flux of radiation by collecting photons,

$$F^{\mathrm{L}}(\nu^{\mathrm{L}})_{|\theta=\theta_{\mathrm{obs}}} = \int_{\substack{\text{(Over observer's plane)}}} I^{\mathrm{L}}(\nu^{\mathrm{L}})_{|R\to\infty, \theta=\theta_{\mathrm{obs}}} \, dS. \tag{7}$$

The disk emits at temperature decreasing as a power-law function of radius. The resulting image is created and plotted, as shown in figure 4. Red colour (prevailing in the left part of the image) corresponds to a decreased energy of incoming photons with respect to energy in the local rest-frame attached to the disk, blue colour (prevailing in the right part of the image) corresponds to an increased energy. Light bending distorts the shape of the disk image, in particular when the observer's inclination is large (here it is almost edge-on, $\theta_{\mathrm{obs}} = 85 \deg$). Notice that the image of the inner edge of the disk is not axially symmetric due to rotation of the black hole (dimensionless angular momentum parameter $a = 0.99$, i.e., almost maximal rotation). This figure is a typical result from computer modelling (Fukue & Yokoyama, 1988; Luminet, 1979; Karas et al., 1992; Viergutz, 1993). The main parameters influencing the final image are the functional dependency of the intrinsic emissivity over the disk surface, $I(r)$, the specific angular momentum a/M of the black hole, and the inclination θ_{obs} of the accretion disk with respect to observer's line of sight.

3. Conclusions

We discussed effects of strong gravity on radiation that propagates from an accretion disk towards a distant observer. Imprints of these effects provide us with a possibility to study black holes residing the center of the disk. Having in mind the applications to present-day X-ray observations, the energy shifts, gravitational lensing and time delays are the principal effects which originate from General Relativity and can be tested. GR effects become dominant in the close vicinity of the hole, where they smear the resulting signal and are responsible for the source spectrum and its variability.

Let us note that the black-hole accretion disk model is defined by a number of parameters. There is a certain degree of degeneracy among the parameter values, so that some parameters cannot be constrained with sufficient confidence. This results in ambiguities that make the fitting procedure difficult. A partial way out is often adopted by freezing some of the parameters at their likely values, however, a more secure solution will require to gather addition observational data about the system.

Polarimetry can be employed to gain additional information. Unlike the case of equatorial (geometrically thin) disk, the possibility of non-negligible vertical thickness introduces an additional degree of freedom. Polarimetric properties are known to be very sensitive to the geometry of the source and we will need this extra piece of information to disentangle GR effects from cumbersome local physics. More complex non-axial geometry of the emitting region needs to be explored, such as spiral waves propagating across the accretion disk and twisted (precessing) disks. Strong gravity near the central black hole is very likely the main agent shaping the overall form of the X-ray spectral features from the inner disk.

References

Chen, K. & Halpern, J. P., Structure of line-emitting accretion disks in active galactic nuclei – ARP 102B. 1989, *Astrophys. J.*, **344**, 115, DOI: 10.1086/167782

Dovčiak, M., Karas, V., & Yaqoob, T., An Extended Scheme for Fitting X-Ray Data with Accretion Disk Spectra in the Strong Gravity Regime. 2004, *Astrophys. J., Suppl.*, **153**, 205, DOI: 10.1086/421115

Eckart, A., Hüttemann, A., Kiefer, C., et al., The Milky Way's Supermassive Black Hole: How Good a Case Is It? 2017, *Foundations of Physics*, **47**, 553, DOI: 10.1007/s10701-017-0079-2

Eracleous, M. & Halpern, J. P., Doubled-peaked emission lines in active galactic nuclei. 1994, *Astrophys. J., Suppl.*, **90**, 1, DOI: 10.1086/191856

Fabian, A. C., Iwasawa, K., Reynolds, C. S., & Young, A. J., Broad Iron Lines in Active Galactic Nuclei. 2000, *Publ. Astron. Soc. Pac.*, **112**, 1145, DOI: 10.1086/316610

Fabian, A. C., Rees, M. J., Stella, L., & White, N. E., X-ray fluorescence from the inner disc in Cygnus X-1. 1989, *Mon. Not. R. Astron. Soc.*, **238**, 729, DOI: 10.1093/mnras/238.3.729

Frank, J., King, A., & Raine, D. 1992, *Accretion power in astrophysics.* (Camb. Astrophys. Ser., Vol. 21)

Fukue, J. & Yokoyama, T., Color photographs of an accretion disk around a black hole. 1988, *Publ. Astron. Soc. Jap.*, **40**, 15

Gerbal, D. & Pelat, D., Profile of a line emitted by an accretion disk - Influence of the geometry upon its shape parameters. 1981, *Astron. Astrophys.*, **95**, 18

Hanni, R. S., Wave fronts near a black hole. 1977, *Phys. Rev. D*, **16**, 933, DOI: 10.1103/PhysRevD.16.933

Karas, V., Theoretical aspects of relativistic spectral features. 2006, *Astronomische Nachrichten*, **327**, 961, DOI: 10.1002/asna.200610672

Karas, V. & Kraus, P., Doppler Tomography of Relativistic Accretion Disks. 1996, *Publ. Astron. Soc. Jap.*, **48**, 771, DOI: 10.1093/pasj/48.5.771

Karas, V., Lanza, A., & Vokrouhlický, D., Emission-line profiles from self-gravitating thin disks. 1995, *Astrophys. J.*, **440**, 108, DOI: 10.1086/175252

Karas, V., Vokrouhlický, D., & Polnarev, A. G., In the vicinity of a rotating black hole - A fast numerical code for computing observational effects. 1992, *Mon. Not. R. Astron. Soc.*, **259**, 569, DOI: 10.1093/mnras/259.3.569

Kato, S., Fukue, J., & Mineshige, S. 2008, *Black-Hole Accretion Disks — Towards a New Paradigm* (Kyoto University Press, Kyoto, Japan)

Kojima, Y., The effects of black hole rotation on line profiles from accretion discs. 1991, *Mon. Not. R. Astron. Soc.*, **250**, 629, DOI: 10.1093/mnras/250.3.629

Kojima, Y. & Fukue, J., Line profiles emitted from an accretion torus. 1992, *Mon. Not. R. Astron. Soc.*, **256**, 679, DOI: 10.1093/mnras/256.4.679

Laor, A., Line profiles from a disk around a rotating black hole. 1991, *Astrophys. J.*, **376**, 90, DOI: 10.1086/170257

Luminet, J.-P., Image of a spherical black hole with thin accretion disk. 1979, *Astron. Astrophys.*, **75**, 228

Murphy, K. D., Yaqoob, T., Karas, V., & Dovčiak, M., On the Prospect of Constraining Black Hole Spin Through X-ray Spectroscopy of Hotspots. 2009, *Astrophys. J.*, **701**, 635, DOI: 10.1088/0004-637X/701/1/635

Viergutz, S. U., Image generation in Kerr geometry. I. Analytical investigations on the stationary emitter-observer problem. 1993, *Astron. Astrophys.*, **272**, 355